

Ax-BxP: Approximate Blocked Computation for Precision-Reconfigurable Deep Neural Network Acceleration

REENA ELANGO VAN, Purdue University, USA

SHUBHAM JAIN, IBM T.J. Watson Research Center, USA

ANAND RAGHUNATHAN, Purdue University, USA

Precision scaling has emerged as a popular technique to optimize the compute and storage requirements of Deep Neural Networks (DNNs). Efforts toward creating ultra-low-precision (sub-8-bit) DNNs for efficient inference suggest that the minimum precision required to achieve a given network-level accuracy varies considerably across networks, and even across layers within a network, requiring support for variable precision in DNN hardware. Previous proposals such as bit-serial hardware incur high overheads, significantly diminishing the benefits of lower precision. To efficiently support precision re-configurability in DNN accelerators, we introduce an approximate computing method wherein DNN computations are performed block-wise (a block is a group of bits) and re-configurability is supported at the granularity of blocks. We propose a framework of approximations to blocked computation that enable efficient re-configurability. We design a DNN accelerator that embodies approximate blocked computation and propose a method to determine a suitable approximation configuration for a given DNN. We achieve 1.17x-1.73x and 1.02x-2.04x improvement in system energy and performance respectively, over an 8-bit fixed-point (FxP8) baseline in various DNNs, with negligible loss in classification accuracy. Further, by varying the approximation configurations at a finer granularity across layers and data-structures within DNNs, we achieve 1.25x-2.42x and 1.07x-2.95x improvement in system energy and performance respectively, with negligible classification accuracy loss.

CCS Concepts: • **Computer systems organization** → **Reconfigurable computing**; • **Computing methodologies** → **Neural networks**; • **Hardware** → **Neural systems**; **Reconfigurable logic applications**.

Additional Key Words and Phrases: Approximate Computing, Precision-Reconfigurable DNN Acceleration

1 INTRODUCTION

Deep Neural Networks (DNNs) have become very popular in recent years due to their ability to achieve state-of-the-art performance in a variety of cognitive tasks such as image classification, speech recognition and natural language processing [1–3]. The remarkable algorithmic performance of DNNs comes with extremely high computation and storage requirements. While these challenges span both training and inference, we focus on the latter scenario where the high computation requirements of DNN inference limit their adoption in energy- and cost-constrained devices [4].

The use of low precision has emerged as a popular technique for realizing DNN inference efficiently in hardware [5, 6]. Lowering the precision or bit-width favorably impacts all facets of energy consumption including computation, interconnect, and memory. State-of-the-art commercial DNN hardware widely supports 8-bit precision for DNN inference, and recent research continues to explore techniques to design networks with even lower precision [7–11].

Recent efforts [7, 12, 13] suggest that realizing ultra-low-precision (sub-8-bit) DNN inference without any accuracy degradation is quite challenging if the precision for all data-structures is scaled uniformly. Therefore, the use of variable precision (across DNNs, and across layers within a DNN) has gained considerable interest. For instance, HAQ [7] shows

Authors' addresses: Reena Elangovan, elangovr@purdue.edu, Purdue University, School of Electrical and Computer Engineering, USA; Shubham Jain, shubham.jain35@ibm.com, IBM T.J. Watson Research Center, Yorktown Heights, NY, USA; Anand Raghunathan, raghunathan@purdue.edu, Purdue University, School of Electrical and Computer Engineering, USA.

that the MobileNet and ResNet DNNs require precision varying from 3 to 8 bits across network layers in order to match the accuracy of a full-precision network.

To support variable precision, one option is to utilize conventional fixed-precision hardware that is provisioned for the worst case precision, possibly gating the unused portions of logic to save power. However, this approach does not fully utilize the potential of aggressive precision-scaling since the unused hardware lowers utilization. Alternatively, variable-precision DNN accelerators with bit-serial [14–16] or bit-fused [17] fabrics have been designed to support re-configurability. However, this re-configurability comes at a high cost as the bit-serial arithmetic circuits incur significant energy and latency overheads with respect to their fixed-precision counterparts of equivalent bit-width, due to multi-cycle operation and control logic [18]. Figure 1 quantifies the energy overhead (at iso-area) incurred while performing 8-bit MAC computations using digit-serial hardware (MAC units) of 2-bits and 4-bits (synthesized to 15nm with Synopsys Design Compiler). As shown, the increased flexibility provided by smaller blocks is accompanied by a much higher energy cost for 8-bit arithmetic. This limits the energy benefits that can be realized from variable-precision DNNs, where bit-width varies from 2-8 bits across layers and across networks [7, 12, 13].

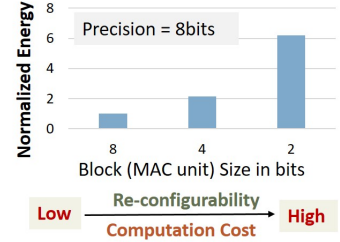


Fig. 1. Computation cost vs re-configurability trade-offs

To design hardware for DNNs that caters to variable precision requirements with minimal overheads, we leverage the intrinsic tolerance of DNNs to approximate computation [19], which is the basis for reduced precision itself [13]. Specifically, we propose Ax-BxP, an approximate computation method to execute DNN inference in which weights and activations are composed of fixed-length blocks (groups of bits), and computations are performed block-wise. Approximate composition of results across blocks is utilized to enable efficient re-configurability at the block granularity. We present a methodology to choose the best approximation configuration for each layer in a DNN. We also propose architectural enhancements to realize Ax-BxP in a standard systolic array based DNN inference accelerator with lightweight design modifications. We show that (i) Ax-BxP with varying approximation configurations across DNNs achieves 1.17x-1.73x and 1.02x-2.04x improvement in system-level energy and performance respectively, and (ii) Ax-BxP with varying approximation configurations across layers within DNNs obtains 1.25x-2.42x and 1.07x-2.95x improvement in system-level energy and performance respectively, in both cases with negligible loss (< 1%) in classification accuracy with respect to an 8-bit fixed-point (FxP) baseline.

2 PRELIMINARIES

2.1 Blocked Fixed Point

Fixed-point (FxP) format is widely used for efficient realization of low-precision DNNs. Blocked fixed-point (BxP) format is an adaptation of the FxP format wherein values are partitioned into fixed-length blocks. In particular, an $(N * K)$ bit signed FxP number X_{FxP} can be represented as a BxP number X_{BxP} with N blocks, each of K bits as shown in Figure 2(a). The blocks of X_{BxP} are arranged in the decreasing order of significance (place value) by default, where the significance of the i_{th} block X_i is 2^{i*K} . We assume a sign-magnitude (two’s complement) representation wherein the most significant bit within the most significant block (X_{N-1}) is the sign bit. The magnitude of X_{BxP} denoted $|X_{BxP}|$, can be derived from its blocks as shown in the figure.

2.2 Blocked Multiplication

Figure 2(b) demonstrates a blocked¹ multiplication between two BxP format numbers X_{BxP} and Y_{BxP} . As shown, each block of X_{BxP} is multiplied with each block of Y_{BxP} to generate N^2 partial products (P). Subsequently, partial products are shifted and accumulated using $N^2 - 1$ additions. Equation 1 expresses an exact blocked multiplication operation, where P_{ij} [$P_{ij} = X_i * Y_j$] represents the partial product of the i^{th} block of X_{BxP} (X_i) and j^{th} block of Y_{BxP} (Y_j).

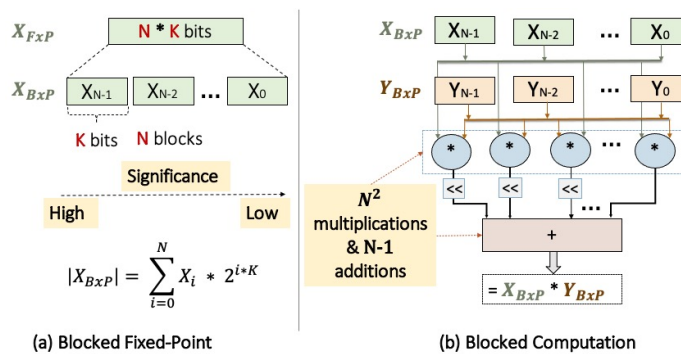


Fig. 2. BxP: Overview

$$X_{BxP} * Y_{BxP} = \sum_{i=0}^{N-1} \sum_{j=0}^{N-1} P_{ij} * 2^{(i+j)*K} \quad (1)$$

3 APPROXIMATE BLOCKED COMPUTATION

In this section, we discuss Ax-BxP, the proposed approximate blocked computation method for designing efficient precision-reconfigurable DNNs. We first detail the key approximation concepts and introduce the Ax-BxP format for representing MAC operands. Subsequently, we present a systematic methodology for designing Ax-BxP DNNs with minimal impact on application-level accuracy. Finally, we demonstrate the integration of Ax-BxP into a standard systolic array-based DNN accelerator using simple hardware enhancements.

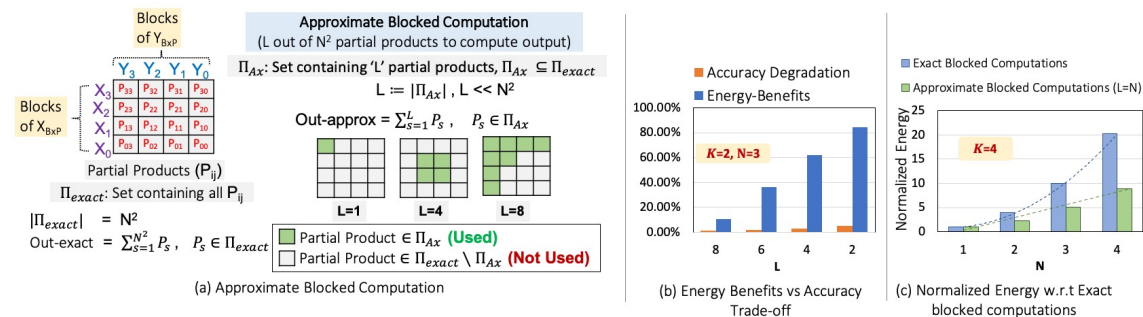


Fig. 3. Approximate blocked computation: Overview

3.1 Approximation Method

The main idea in Ax-BxP is to perform blocked computations by selecting a subset of partial products (out of the total of N^2). Figure 3(a) illustrates the concept, where the multiplication of operands (X_{BxP} and Y_{BxP}) is performed by computing and accumulating only $L = |\Pi_{Ax}|$ out of N^2 possible partial product terms. Formally (as shown in

¹Blocked multiplication is also known in the literature as digit serial multiplication (e.g., [20]) and bit-level composable multiplication (e.g., [17]).

Figure 3(a)), we characterize Ax-BxP multiplication using a set $\Pi_{Ax} \subseteq \Pi_{Exact}$, wherein the final output (out-approx) is given by summing the partial products (P_s) in Π_{Ax} . Ax-BxP involves two key design choices – (i) L (the size of set Π_{Ax}) and (ii) the choice of elements (partial products) within the set Π_{Ax} . These design choices affect both the computational errors introduced and the energy benefits, and therefore need to be explored judiciously to produce the best possible energy-accuracy trade-offs.

Figure 3(b) presents the energy-accuracy tradeoff provided by Ax-BxP for the AlexNet DNN on the CIFAR10 dataset, across various choices of L with fixed values of N and K (i.e., $K = 2, N = 3$, with $L = 9$ corresponding to exact blocked computation). As L decreases, the accuracy decreases minimally, whereas the energy benefits increase drastically. The computational accuracy reported is for the best choice of Π_{Ax} among all choices of Π_{Ax} , identified using the methodology described in Section 3.3. To estimate energy benefits, we synthesized the exact and approximate RTL designs (described in Section 3.4) to the 15nm technology node using Synopsys Design Compiler. The results suggest a favorable energy-accuracy trade-off, which arises due to the typical data distribution seen in DNNs [11], wherein a majority (>90%) of the operations can be computed accurately at low-precision, but computing the remaining operations at higher precision is critical to preserving accuracy. We also evaluated the energy benefit across various values of N by fixing the values of K and L ($K=4, L=N$). As shown in Figure 3(c), the energy of approximate block-wise computations increase linearly with N as we require $O(N)$ block-wise partial products to be evaluated and accumulated. In contrast, the energy of exact blocked computation increases quadratically as it requires $O(N^2)$ block-wise partial products.

For a given L , when fewer than N blocks of X_{BxP} or Y_{BxP} (or both) are used to construct Π_{Ax} , we can achieve memory footprint savings in addition to computation savings by storing only the required blocks. To leverage this, we introduce a new Ax-BxP tensor format for storing the Ax-BxP operands in the following sub-section. Section 3.3 describes the *significance-* and *value-based* methods that we use for choosing the required blocks of the operands.

3.2 Ax-BxP Tensor

We introduce a new format for storing Ax-BxP operand blocks and their indices. The Ax-BxP format uses the following fields – (i) total number of blocks (N), (ii) block-size (K), (iii) the set \mathcal{I} containing indices of the operand blocks chosen for Ax-BxP computation, (iv) number of chosen blocks ($\tilde{N} := |\mathcal{I}| \leq N$) and (v) data blocks (*data*), which are arranged in decreasing order of significance. The size of *data* is $\tilde{N} * K$ bits. Note that, during exact blocked computation, $\tilde{N} = N$ and \mathcal{I} is not required.

We define an Ax-BxP Tensor as a tensor (typically, the weights or activations of an entire layer) composed of scalar elements in the Ax-BxP Format, where the elements share common values of the parameters (*viz.*, $N, K, \tilde{N}, \mathcal{I}$). Ax-BxP Tensor is presented as a template class in Figure 4, which also illustrates the memory layout of the different fields. Since the space required to store the parameters are amortized across an entire tensor, the associated memory footprint is negligible. Furthermore, when $\tilde{N} < N$ the size of the *data* field is reduced, resulting in savings in memory footprint and memory traffic in addition to computation.

```

Ax-BxP Tensor <Template T1>{
  int8 K; // #bits per block
  int8 N; // #blocks
  int8  $\tilde{N}$ ; // #chosen blocks ( $\tilde{N} \leq N$ )
  int8* I; // set of indices of  $\tilde{N}$ 
  vector<int> shape; // shape
  T1* data; // blocks of data
};

```

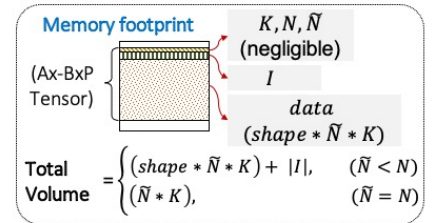


Fig. 4. Ax-BxP Tensor: Memory Layout

3.3 Design Methodology

Next, we present key design considerations involved in approximating DNNs using Ax-BxP and the methodology we use to select the Ax-BxP format for each layer in the network. In this subsection, we first characterize the Ax-BxP design space. Subsequently, we provide pruning techniques to reduce the complexity of the design space exploration and algorithms for systematically designing Ax-BxP DNNs.

3.3.1 Design Space Characterization. For a given bit-width (BW), where $BW = N * K$, an Ax-BxP MAC operation (characterized by the set Π_{Ax}) can be designed in numerous ways. We define Ω as a set enumerating all possible ways of constructing Π_{Ax} . Equation 2 expresses the size of Ω ($|\Omega|$) which is determined by free variables L and N. As shown, for a given BW, we are free to choose N (i.e., number of blocks) to be an integer from 1 to BW. Subsequently, we can select the approximation-level by determining L, i.e., number of partial products to be used during MAC operations. The value of L can be 1 to N^2 , where $L=N^2$ represents an exact blocked computation. Lastly, there are $\binom{N^2}{L}$ ways of selecting L out of N^2 partial products.

$$|\Omega| = \sum_{N=1}^{BW} \sum_{L=1}^{N^2} \binom{N^2}{L} \quad (2)$$

3.3.2 Design Space Constraints. To reduce the search space $|\Omega|$ which is exponential in N, we put forth the following arguments to bound $|\Omega|$ by constraining BW, K, N, and L:

- **Bitwidth (BW):** Since a bit-width of 8 for both activations and weights is sufficient to preserve accuracy during inference [21], we constraint $BW \leq 8$.
- **Bits in a block (K):** We also bound K such that $1 < K \leq 4$. By setting $K > 1$, we avoid the latency and energy overheads associated with bit-serial (K=1) implementation [17]. Moreover, we introduce an upper-bound on K ($K \leq 4$) to avoid $N = 1$ (i.e., an FxP implementation).
- **Number of Blocks (N):** We set N as $N = \lceil BW/K \rceil$. Therefore, for $BW \leq 8$ and $1 < K \leq 4$, the allowed values of N are 2,3 and 4.
- **Size of set Π_{Ax} (L):** Lastly, we constraint $L \leq N$ based on the energy-accuracy trade-offs discussed in Section 3.1 and shown in Figure 3. We found that $L \leq N$ provides ample design choices, wherein we can obtain significant energy benefits with minimal impact on computational accuracy. Apart from reduction in design space, bounding $L \leq N$ also helps in minimizing the design complexity of both the control logic and Ax-BxP PEs at the systolic-array level, mitigating the associated reconfiguration overheads (discussed further in Section 3.4).

Equation 3 expresses the size of reduced design space (Ω_c) obtained after constraining the variables BW, K, N, and L.

$$|\Omega_c| = \sum_{N=2,3,4} \sum_{L=1}^N \binom{N^2}{L} \quad (3)$$

Using numerical methods, we evaluate $|\Omega_c|$ to be 2655 for a single DNN layer. For a DNN with n layers, $|\Omega_c| = 2655^n$. This is a large size for practical design space exploration, especially since re-training is needed to alleviate the accuracy degradation caused by approximation. Motivated by this, we prune the search space by eliminating several sub-optimal Ax-BxP configurations.

3.3.3 Design Space Pruning. We prune the search space by restricting the contents of the set Π_{Ax} for a given L. Figure 5 illustrates the possible choices of Π_{Ax} , wherein W_{BxP} and A_{BxP} are the Ax-BxP weight and activation tensors,

respectively, of a DNN layer. Further, \tilde{N}_W (\tilde{N}_A) and \mathcal{I}_W (\mathcal{I}_A) represent number of blocks and block indices respectively, of W_{BxP} (A_{BxP}) used for computing the MAC operation ($W_{BxP} * A_{BxP}$). As shown, there are a variety of ways of choosing 4 (L) out of 16 (N^2) partial products. The selected partial products (shown in green) cast a shape on the 2D array that represents all possible N^2 partial products. The shape could be scattered, irregular, or regular. In our design exploration, we restrict to regular shapes that substantially reduces the search space complexity. Formally, restricting to regular shapes constraints L as shown in Equation 4.

$$L = \tilde{N}_W * \tilde{N}_A. \quad (4)$$

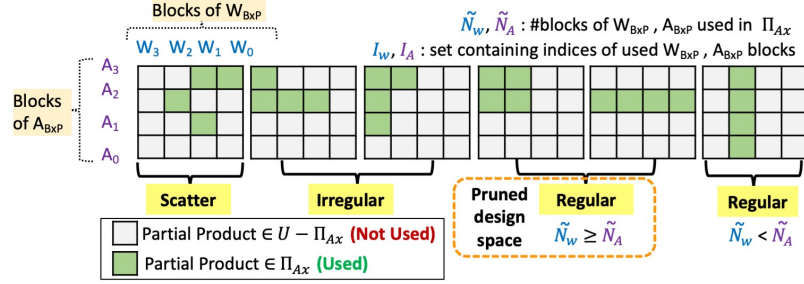


Fig. 5. Design search space for L=4, N=4: Illustration

Based on previous studies that show activations to be more sensitive to precision-scaling than weights during DNN inference operations [10, 21], we further prune the search space such that $\tilde{N}_A \geq \tilde{N}_W$. In other words, we never select configurations (e.g., the right most configuration in Figure 5), wherein a weight operand (W_{BxP}) has more blocks than an activation operand (A_{BxP}). Equation 5 show the size of the design search space (Ω_{c+p}) obtained after pruning, wherein $\binom{N}{\tilde{N}_W}$ and $\binom{N}{\tilde{N}_A}$ are the number of possible ways of selecting \tilde{N}_W and \tilde{N}_A blocks, respectively, out of N blocks. It is worth mentioning that although Equation 5 restricts the number of choices of Π_{Ax} , it enables an efficient systolic array implementation so that we can retain the benefits achieved using Ax-BxP at system-level due to reduced computation, memory footprint and memory traffic.

$$|\Omega_{c+p}| = \sum_{N=2,3,4} \sum_{\tilde{N}_A=1}^N \sum_{\tilde{N}_W=1}^{\tilde{N}_A} \binom{N}{\tilde{N}_A} \binom{N}{\tilde{N}_W} \quad (5)$$

3.3.4 Design heuristics. Next, we present the two heuristics, viz., *static-idx* and *dynamic-idx*, to select \tilde{N}_W (\tilde{N}_A) blocks of W_{BxP} (A_{BxP}).

In the *static-idx* heuristic, the operand blocks are chosen in a *significance-aware* manner where the blocks of higher significance are always chosen over the blocks of lower significance. For a given \tilde{N} , we first find the index of the most-significant non-zero block of the operand tensor and choose the next \tilde{N} consecutive blocks in the decreasing order of significance. Since the blocks of data in the *data* field of the Ax-BxP tensor are arranged in the decreasing order of significance by default, we require only the start index ($\mathcal{I}[N-1]$) or the end index ($\mathcal{I}[0]$) to determine the indices of all the blocks. Recall that \mathcal{I} is common to all the scalar elements of an operand tensor.

Note that when \mathcal{I} is chosen using the *static-idx* heuristic, the small-valued scalar elements in an operand tensor cannot be represented with sufficient resolution. For instance, consider the activation histogram (generated using ImageNet dataset) of a quantized AlexNet layer shown in Figure 6, where the activation values are represented using 2 blocks of 4 bits each, (i.e $N = 2, K = 4$). In the histogram, both blocks may be non-zero for large values that reside in bins $[1,3]$, whereas only the least significant block is non-zero for the values in bins $[-4,-1]$. Therefore, when $\tilde{N} = 1$, *static-idx* heuristic chooses the most significant block for each scalar element, the small values in bins $[-4,-1]$ are approximated to zero. To represent the smaller scalar values with high resolution, we introduce *dynamic-idx* heuristic, where the set \mathcal{I} is chosen specifically for each scalar element in a tensor.

In the *dynamic-idx* heuristic, the distribution of the scalar values (of a tensor) in different blocks is used in determining the set \mathcal{I} (i.e., the index of the most significant block). Subsequently, each scalar is represented using \tilde{N} consecutive blocks starting from it's most-significant non-zero block. Note that the dynamic choice heuristic is based on both significance and value of the blocks. Figure 7 quantifies the advantage of *dynamic-idx* heuristic over the *static-idx* by showing the obtained error distribution (obtained using ImageNet dataset) on an Alexnet layer. As shown, *dynamic-idx* can achieve much lower error rate in comparison to *static-idx* heuristic. It is worth mentioning that the block indices in the set \mathcal{I} could be chosen in a non-contiguous manner. However, we observe that adopting non-contiguous blocks show no advantage in representing DNN data-structures and can lead to considerable control logic overhead. Further, as previously mentioned, when contiguous blocks are chosen, $|\mathcal{I}| = 1$, as we just need to store the index of the most significant block. Memory saving is less for *dynamic-idx* heuristic in comparison to *static-idx* heuristic, as we need to store \mathcal{I} for each scalar. For a given N and \tilde{N} , the overhead of appending \mathcal{I} to each data element is $\lceil \log_2((N - \tilde{N}) + 1) \rceil$ bits. For example, if $K=2, N=4, \tilde{N}=2$, we have 2 additional bits (for index in \mathcal{I}) every 4 ($K \cdot \tilde{N}$) compute bits. Therefore, the overall memory footprint decreases by $\sim 25\%$ (from 8 bits to 6 bits).

Since L and the set Π_{Ax} can be derived for a given K, \tilde{N}_W and \tilde{N}_A , the design space Ω can now be re-characterized as a set of all 3-tuples $\{K, \tilde{N}_W, \tilde{N}_A\}$ that satisfy all the constraints discussed thus far. The Ax-BxP configurations in Ω are listed against the block-size K in Table 1. Furthermore, we define two modes of Ax-BxP *Static* and *Dynamic* where the operand blocks are chosen using the *static-idx* heuristic and the *dynamic-idx* heuristic respectively.

Table 1. Design Space for approximate blocked computation

Block-size	Ax-BxP configuration = $\{(K, \tilde{N}_W, \tilde{N}_A)\}$
$K = 2$	$\{(2,1,4), (2,1,3), (2,2,2), (2,1,2), (2,1,1)\}$
$K = 3$	$\{(3,1,3), (3,1,2), (3,1,1)\}$
$K = 4$	$\{(4,1,2), (4,1,1)\}$

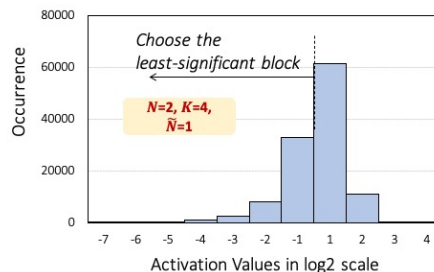


Fig. 6. Significance of the non-zero activation blocks in a layer of quantized AlexNet

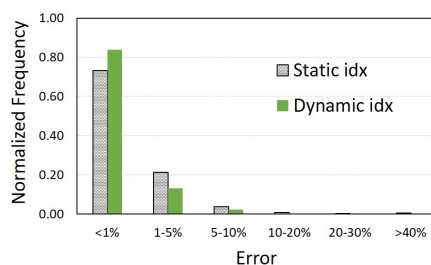


Fig. 7. Operand blocks selection heuristics: Error Analysis

3.3.5 *Designing DNNs using Ax-BxP.* We now present a systematic methodology to design DNNs using Ax-BxP. Algorithm 1 describes the pseudo code that we utilize to identify best Ax-BxP configuration for each data-structure of each DNN layer. It takes a pre-trained DNN model (DNN_{Fxp}), a training dataset (Tr_{data}), a target block size (K_{tgt}), and a limit on allowed accuracy degradation (γ) as inputs and produces Ax-BxP DNN (DNN_{AxBxP}) as an output. We first utilize Tr_{data} to evaluate the baseline network accuracy (line 4) and construct data-value histograms ($DsHist_{list}$) of each data-structure within the network (line 5). Next, we identify the best Ax-BxP configuration for a DNN layer using the histograms of the associated weight (W_{Fxp}) and activation (A_{Fxp}) pair (lines 6-12). As detailed in Algorithm 1, to obtain best Ax-BxP configuration, we first form a pruned search space (Ω_{c+p}) (line 7), and subsequently, explore the choices within Ω_{c+p} to find the best Ax-BxP configuration which is represented by $N_W, \tilde{N}_W, N_A,$ and \tilde{N}_A (line 8). Next, data-structures are converted to Ax-BxP tensor using the Convert-To-AxBxP function (lines 9-10) and inserted into DNN_{AxBxP} network (line 11). Once all data-structures are converted to Ax-BxP tensor, we re-train DNN_{AxBxP} until the network accuracy is within the desired degradation limit ($< \gamma$) or the maximum allowed trained epochs (maxEpoch) is exceeded.

Algorithm 1: Designing AxBxP DNN

```

1: Input:{ $DNN_{Fxp}$ : Pre-trained FxP DNN,  $Tr_{data}$ : Training dataset,  $\gamma$ : Max Accuracy Loss,  $K_{tgt}$ : Target block size}
2: OUTPUT: Approximate Blocked DNN
3:  $DNN_{AxBxP} = DNN_{Fxp}$  /* initialize */
4:  $Acc_{Fxp} = \text{computeAccuracy}(DNN_{Fxp})$ 
5:  $DsHist_{list} = \text{getDist}(DNN_{Fxp}, Tr_{data}) \forall \text{ datastructures}$ 
6: for each [Weight ( $W_{Fxp}$ ), Activations ( $A_{Fxp}$ )] pair  $\in DsHist_{list}$ 
7:    $\Omega_{c+p} = \text{formPrunedSearchSpace}(W_{Fxp}, A_{Fxp}, K_{tgt})$  /* Searching best AxBxP configuration */
8:    $(N_W, \tilde{N}_W, N_A, \tilde{N}_A) = \text{getBestConfig}(\Omega_{c+p}, DNN_{AxBxP}, K_{tgt}, \gamma)$ 
9:    $W_{AxBxP} = \text{Convert-To-AxBxP}(W_{Fxp}, N_W, \tilde{N}_W, K_{tgt})$ 
10:   $A_{AxBxP} = \text{Convert-To-AxBxP}(A_{Fxp}, N_A, \tilde{N}_A, K_{tgt})$ 
11:  insert-AxBxP-Tensors ( $DNN_{AxBxP}, W_{AxBxP}, A_{AxBxP}$ )
12: end for
13: numEpochs=0/* Re-train */
14: while  $\gamma < (Acc_{Fxp} - \text{computeAccuracy}(DNN_{AxBxP}))$  and numEpochs < maxEpoch )
15:   AxBxP-Aware-Training ( $DNN_{AxBxP}, Tr_{data}$ )
16:   numEpochs++
17: return  $DNN_{AxBxP}$ 

```

Algorithm 2: getBestConfig

```

1: Input: { $\Omega_{c+p}$ : Pruned Design Space,  $DNN_{AxBxP}$ ,  $K_{tgt}$ : Target block size,  $\gamma$ : Max Accuracy Loss}
2: OUTPUT: Best AxBxP Config
3: while  $\gamma < (Acc_{Fxp} - Acc_{AxBxP})$ 
4:   AxBxP-config =  $\Omega_{c+p}.\text{pop}()$ 
5:   Convert-and-insert-AxBxP-Tensors ( $DNN_{AxBxP}, W_{AxBxP}, A_{AxBxP}, \text{AxBxP-config}$ )
6:    $Acc_{AxBxP} = \text{evaluate}(DNN_{AxBxP})$ 
7: return AxBxP-config

```

We determine the best AxBxP configuration layer by layer for a given DNN as shown in Algorithm 1 (lines 6-12). We start with a pre-trained DNN_{Fxp} , where exact computations are performed in each layer. Once we find the best

Algorithm 3: Convert-To-AxBxP

- 1: **Input:** $\{X_{Fxp}$: FxP tensor, (K, N_X, \tilde{N}_X) : Ax-BxP configuration}
 - 2: **OUTPUT:** Ax-BxP tensor
 - 3: **For each** scalar x in X_{Fxp}
 - 4: $Block_{list} = \text{Get-Significance-Sorted-Blocks}(x, K, N_X)$
 - 5: $I_x = \text{get-idx-first-Non-Zero-block}(Block_{list})$
 - 6: $X_{AxFxp} = \text{pick-insert-Blocks-in-Range}(I_x, I_x, \tilde{N}_X)$
 - 7: **return** X_{AxBxp}
-

AxBxP configuration for a layer, we convert the operands of that layer to AxBxP format and proceed to the next layer. Algorithm 2 describes the methodology to choose the best AxBxP config for a given layer of DNN, block-size K_{tgt} and target accuracy degradation γ . We set the operands to each of the AxBxP formats in Ω_{c+p} (lines 4-5), and evaluate the resulting DNN_{AxBxp} (line 6). We perform the evaluation in a subset of the training dataset to speed-up the search. During evaluation, we perform re-training for 1 epoch in 120,000 images followed by testing in 5000 images to determine accuracy. Subsequently, we choose the AxBxP configuration that provides the desired accuracy (line 7).

We note that after the pruning of design-space described in section 3.3.3, the design-space for finding the best approximation configuration is drastically reduced to 2, 3 and 5 choices per layer for $K = 4, 3$ and 2 , respectively. Since we perform a greedy search on a layer-by-layer basis, the size of the pruned design space for a DNN with N layers is upto $5N$. For C choices, DNN with N layers and evaluation time of T seconds the time taken to find the best DNN_{AxBxp} is CNT .

Algorithm 3 outlines the pseudo code for converting FxP tensors to Ax-BxP tensors using dynamic-idx heuristic. It takes an FxP tensor (X_{Fxp}) and Ax-BxP configuration (K, N_X, \tilde{N}_X) as inputs and produces an Ax-BxP tensor (X_{AxBxp}) as output. A key function of this algorithm is to determine indexes (I_x) of the chosen blocks. To achieve this objective, we first convert fixed point scalars to blocked fixed-point scalars (line 2) and subsequently, pick \tilde{N}_X contiguous blocks starting from the first non-zero block. Next, the chosen blocks and indexes are inserted into the Ax-BxP tensor (line 4). After all scalars have been converted X_{AxBxp} tensor is returned (line 5).

3.4 Ax-BxP DNN Accelerator

Figure 8 shows the proposed Ax-BxP DNN accelerator, which is a conventional systolic-array based DNN accelerator with enhancements such as Ax-BxP PE, control logic and peripheral units (ToAx-BxP) to support Ax-BxP computation. We design the Ax-BxP DNN accelerator for a fixed K (although k is a parameter in the RTL, it is specified at synthesis time). While the proposed approach can be applied with any

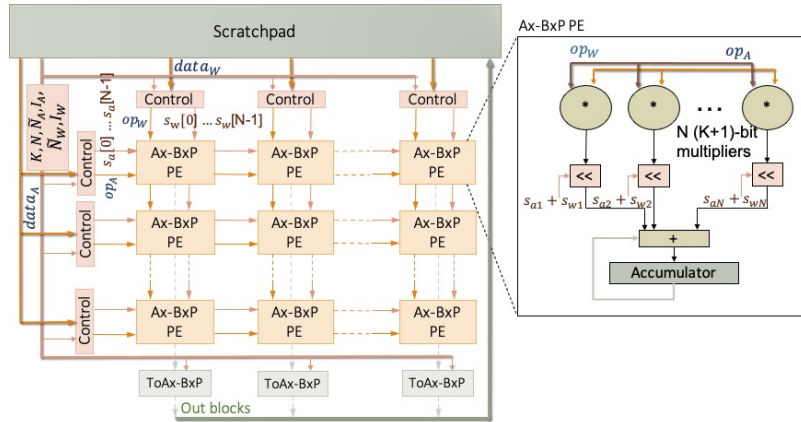


Fig. 8. Ax-BxP Accelerator

DNN dataflow, for illustration we focus on output stationary dataflow. The control logic partitions the Ax-BxP operands into blocks and determines the corresponding shift-amounts. These operand blocks and shift amounts are used to perform the Ax-BxP MAC operations in the Ax-BxP PEs. Finally, the output activations computed by the Ax-BxP PEs are converted into the Ax-BxP format by the ToAx-BxP logic, using the methodology described in Algorithm 3 (see Section 3.3.5). We now discuss the design of the *Ax-BxP PE* and the *Control* logic in detail.

3.4.1 Ax-BxP Processing Element (Ax-BxP PE). The Ax-BxP PEs contain $N = \lceil 8/K \rceil K + 1$ bit signed multipliers and N shifters to support the Ax-BxP computations. The partial products generated by the multipliers are shifted by the shift amounts determined by the control logic, and are accumulated at high-precision in the accumulator to generate the output activations. It is worth noting that as L decreases, the throughput achieved by Ax-BxP PEs increases since a fixed number (N) of multiplications are performed in each cycle.

For a given K and a given mode of Ax-BxP, Ax-BxP PEs support all the Ax-BxP configurations in Ω_{c+p} with block size K by allowing different shift amounts. The different shift amounts are realized in the shifters using multiplexers. The number of multiplexers increases with the number of unique shift amounts to be supported, resulting in increases in energy and area overheads. It is straightforward to show that larger number of unique shift amounts must be supported by the Ax-BxP PE during dynamic Ax-BxP compared to static Ax-BxP. Therefore, the energy and area of Ax-BxP PEs are comparatively lower during the static mode.

3.4.2 Control. The control logic blocks in the Ax-BxP accelerator partition A_{AxBxP} and W_{AxBxP} into signed blocks of $K + 1$ bits each, and determine the shift amounts corresponding to each of these blocks. For instance, as shown in figure 8, W_{AxBxP} is partitioned into blocks $op_W = W_0, \dots, W_{N-1}$ and the corresponding shift amounts $s_w[0], \dots, s_w[N - 1]$ are computed. The shift amounts are determined based on the index of the operand blocks, where the shift amount corresponding to the i^{th} block of both A_{AxBxP} and W_{AxBxP} is computed as $i * K$. The control logic derives the operand block indices for A_{AxBxP} (W_{AxBxP}) from \bar{I}_A and \tilde{N}_A (\bar{I}_W and \tilde{N}_W) as discussed in section 3.3.4. Note that during the static-mode, the parameters \bar{I}_A , \bar{I}_W , \tilde{N}_A and \tilde{N}_W are fixed for the scalar operands in a layer and therefore, are broadcast to the control blocks at the start of a layer’s computations. During dynamic-mode, the control logic obtains \bar{I}_A and \bar{I}_W from the scalar elements of A_{AxBxP} and W_{AxBxP} , respectively. It is worth noting that the design complexity of both the Ax-BxP PEs and the control logic depends on the number of unique shift amounts to be supported which in-turn depends on L . Therefore, constraining L to be $\leq N$ minimizes the design complexity while preserving the classification accuracy (as shown in section 5).

4 EXPERIMENTAL METHODOLOGY

In this section, we present the experimental methodology used to evaluate Ax-BxP.

Accuracy Evaluation: We evaluate Ax-BxP using three state-of-the-art image recognition DNNs for the ImageNet dataset, *viz.* ResNet50, MobileNetV2 and AlexNet. We perform upto 5 epochs of re-training for all the Ax-BxP configurations considered. The ImageNet dataset has 1.28M training images and 50,000 test images. We use the entire test dataset for the accuracy evaluation. We use an Intel Core i7 system with NVIDIA GeForce 2080 (Turing) graphics card for the simulations.

System Energy and Performance Evaluation: We design the Ax-BxP DNN accelerator by expanding the conventional systolic array accelerator modelled in ScaleSim [22] to include enhancements such as Control logic, ToAxBxP logic and the AxBxP PEs, all synthesized to the 15nm technology node using Synopsys Design Compiler. We consider an output-stationary systolic array of size 32x32 and on-chip scratch-pad memory of 2MB operating at 1GHz. The

on-chip memory is modelled using CACTI [23]. We design our baseline FxP8 accelerator, also synthesized to the 15nm technology node using Synopsys Design Compiler, as a conventional systolic array with FxP8 PEs that can implement 8-bit MAC operations. The system-level energy and performance benefits of the Ax-BxP accelerator are evaluated against the FxP8 accelerator. To evaluate the benefits over mixed-precision quantization, we adopt the HAQ [7] precision configuration and we design a power-gated FxP8 baseline with power-gated FxP8 PEs, i.e, we design the PEs for the worst-case precision of 8 bits and power-gate the unused portions during low-precision computations. Additionally, we evaluate the system benefits of the proposed Ax-BxP in the Bit-Fusion accelerator [17].

5 RESULTS

In this section, we demonstrate the energy and performance benefits of Ax-BxP over exact computations at the PE-level and system level using the proposed Ax-BxP DNN accelerator. Additionally, we also demonstrate the benefits of Ax-BxP in the Bit-Fusion [17] accelerator.

5.1 PE-level Energy and Area Benefits

Figure 9 shows the energy and area benefits of the AxBxP PE for $K = 2, 3, 4$ w.r.t FxP8 PE. On an average, the energy and area benefits of AxBxP PE in dynamic mode are 1.69x and 1.12x, respectively. In static mode, the average energy and area benefits are 1.87x and 1.25x, respectively.

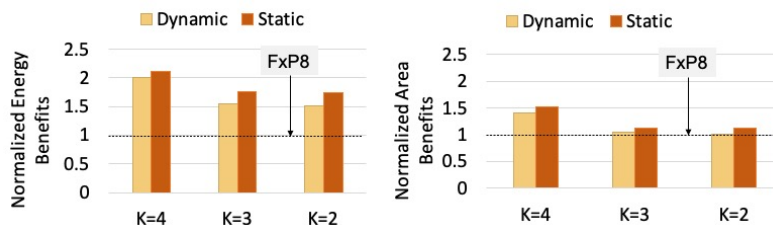


Fig. 9. Computation Energy and Area Benefits w.r.t. FxP8 baseline

Recall from section 3.4 that for a given K , the Ax-BxP PEs can support any Ax-BxP configuration by allowing shifts by different amounts. The energy and area overheads of Ax-BxP PEs increase with an increase in the number of unique shift amounts to be supported. The number of unique shift amounts to be supported are proportional to $N = \lceil 8/K \rceil$. Therefore the energy benefits decrease as K decreases during both static and dynamic Ax-BxP. Furthermore, since greater number of shift amounts are to be supported for the dynamic mode, the energy benefits during dynamic Ax-BxP are lower than static Ax-BxP for all K . Figure 10 (left) shows the energy breakdown of multipliers, shifters and adders, and the accumulator in Ax-BxP PEs for all K in both static and dynamic modes of Ax-BxP. For approximately equal multiplier and accumulator energy, we observe that the overhead due to re-configurability (i.e shifters and adders) is greater in dynamic mode vs static mode. Figure 10 (right) shows the area breakdown of the Ax-BxP PEs and the FxP8 PE. Similar to energy, we find that for a given K , the re-configurability overhead is greater in dynamic vs static mode. The energy and area overheads of re-configurability are larger for smaller K because of the greater number of shift amounts to be supported.

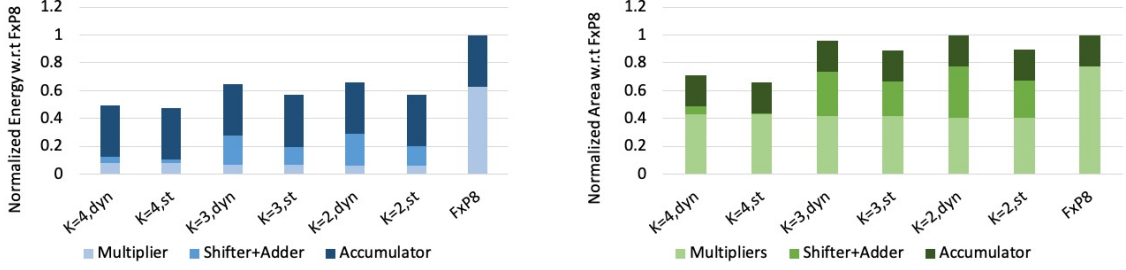


Fig. 10. Computation Energy Breakdown (left) and Area Breakdown (right) w.r.t. FxP8 baseline

5.2 System Benefits and ImageNet Accuracy of dynamic Ax-BxP with varying config. across DNNs

Figure 11 shows the system-level benefits of dynamic Ax-BxP inference compared to the FxP8 baseline at iso-area. We find that the best Ax-BxP configuration in Ω_{c+p} for a given K , *i.e.* the configuration that provides maximum energy benefits with minimum accuracy loss ($< 1\%$), varies across the networks considered. For a given network, we maintain the Ax-BxP configurations uniform across its layers.

Table 2. Best Dynamic Ax-BxP configurations

Block-size	AlexNet	ResNet50	MobileNetV2
$K = 4$	(4,1,1)	(4,1,2)	(4,1,2)
$K = 3$	(3,1,1)	(3,1,2)	(3,1,2)
$K = 2$	(2,1,2)	(2,1,2)	(2,2,2)

Table 2 shows the best Ax-BxP configuration for a given K and network. The proposed Ax-BxP DNN accelerator efficiently supports varying Ax-BxP configurations across networks and achieves system-level energy reduction of 1.2x-1.87x, 1.02x-1.92x and 1.13x-2.48x for $K = 4, 3$ and 2, respectively compared to the FxP8 baseline. Figure 11 shows the breakdown of the normalized system-energy into Off-Chip memory access energy, On-Chip Buffer access energy and the Systolic-Array energy. We achieve a significant reduction in each of these components in our proposed Ax-BxP accelerator across DNNs and the approximation configurations considered.

The 1.04x-5.08x reduction in the systolic-array energy is primarily from the Ax-BxP PE benefits discussed in section 5.1. Additionally, for a given K , when L decreases, the throughput of the Ax-BxP DNN accelerator increases as discussed in section 3.4. Therefore, the overall inference cycles reduces, resulting in further reduction in the systolic-array energy. However, the Imagenet classification accuracy decreases with a decrease in L . Furthermore, by selecting to store a subset of the operand blocks, we achieve 1.01x-1.6x and 1.03x-2.36x reduction in On-chip and Off-chip memory access energy, respectively. For a given K , the memory-access energy decreases as L decreases. This is because of the reduction in memory footprint and the number of accesses despite the overhead of storing the $\lceil \log_2((N - \tilde{N}) + 1) \rceil$ bits of operand block indices during dynamic Ax-BxP.

The performance benefits during dynamic Ax-BxP compared to FxP8 at iso-area are shown in Figure 11. We obtain 1.29x-2.66x, 1.09x-3.1x and 1.02x-4.06x performance benefits for $K = 4, 3$ and 2, respectively for the configurations listed in Table 2. For a given K , smaller L results in increased throughput which results in increased performance.

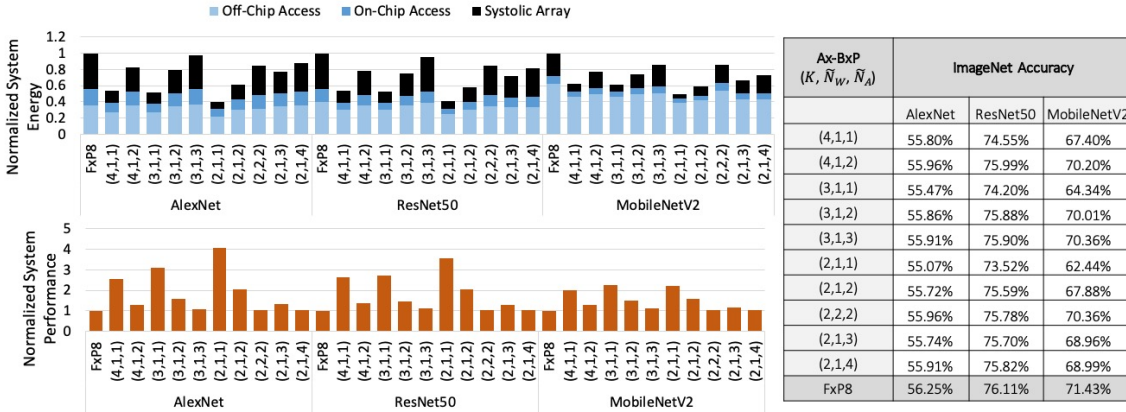


Fig. 11. System-level Benefits with dynamic Ax-BxP

5.3 System-level Energy Benefits and ImageNet Accuracy with varying Ax-BxP configurations within DNNs

The benefits of Ax-BxP can be further highlighted in the context of variable-precision DNNs that have different layer-wise precision requirements. The uniform Ax-BxP configuration of (2, 1, 1) provides the maximum system benefits. However, it suffers from significant accuracy degradation. To improve the classification accuracy and to maximize the system-benefits, we vary the precision in a coarse-grained manner across the layers of these DNNs with $K = 2$. We use the Ax-BxP configurations (2, 1, 2) and (2, 1, 1) for ResNet50 and AlexNet, and (2, 2, 2) and (2, 1, 2) for MobileNetV2. The layer-wise precision configurations considered are shown in Figure 12. We achieve 1.25x-2.42x reduction in system energy and 1.07x-2.95x improvement in system performance compared to FxP8 baseline with negligible loss in classification accuracy.

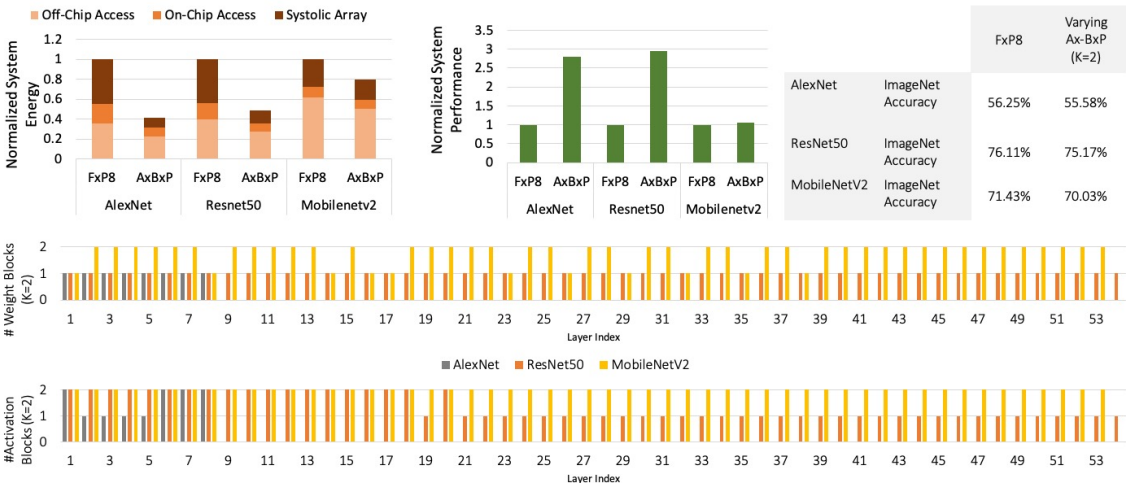


Fig. 12. System-level benefits and ImageNet accuracy for mixed-precision networks

Additionally, we compare the proposed AxBxP against the HAQ [7] mixed-precision configuration. We implement the HAQ configuration (shown in Figure 13) in a conventional systolic array accelerator with power-gated PEs, i.e, we design the PEs to support the worst-case precision of 8-bits and power-gate the unused portions during sub-8-bit computations. Figure 13 shows the normalized system-energy breakdown, performance, and ImageNet accuracy of AxBxP and HAQ implementations. We observe that AxBxP achieves 1.02x-1.69x system-energy reduction and 1.07x-2.95x performance improvement compared to HAQ. The memory access energy (off-chip + on-chip) of AxBxP is 0.95x and 1.05x of the HAQ memory-access energy for ResNet50 and MobileNetV2, respectively. The small overhead in case of MobileNetV2 is caused by storing the AxBxP operand block indices. Despite this overhead, AxBxP achieves superior system benefits compared to HAQ by substantially reducing (1.24x-3.5x) the systolic-array energy. This is the result of lower overall inference cycles of the AxBxP, achieved by superior systolic-array utilization compared to the power-gated FxP8 implementation of HAQ. As shown in Figure 13, HAQ does not provide any performance improvement compared to FxP8 because the power-gated PEs cannot increase the throughput of the systolic-array.

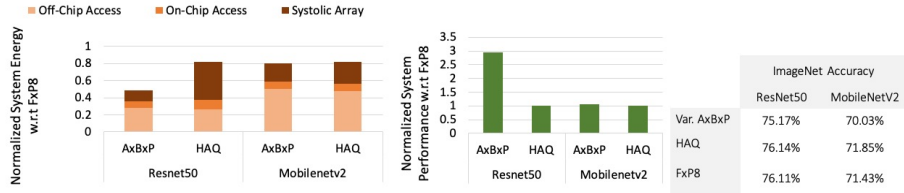


Fig. 13. Comparison to HAQ precision configuration implemented in a power-gated FxP8 systolic array

5.4 Benefits of AxBxP in the Bit-Fusion Accelerator

The energy and performance benefits of dynamic Ax-BxP in the Bit-Fusion accelerator compared to exact computations, is shown in Figure 14. We have considered the Ax-BxP configurations with $K = 2$, since the bit-bricks in Bit-Fusion PE are designed for a block-size of 2. By performing approximations using Ax-BxP, we could achieve energy benefits upto 3.9x and performance benefits upto 12.3x in the Bit-Fusion accelerator. The Bit-Fusion PEs achieve a comparatively higher throughput for a given L . The increase in throughput is as high as 16x when $L = 1$, resulting in the 12.3x benefits for the configuration (2, 1, 1).

5.5 System Benefits and ImageNet Accuracy of static Ax-BxP

Figure 15 shows the system benefits of static Ax-BxP compared to the FxP8 baseline at iso-area. The energy benefits during static Ax-BxP are greater than the dynamic Ax-BxP across networks and across configurations. This is because the AxBxP PEs are simpler in terms of the number of shift amounts to be supported during the static mode, compared to the dynamic mode. Furthermore, the memory footprint of the operands are lower during static mode compared to the dynamic mode, since the cost of storing and fetching \bar{I}_W and \bar{I}_A are amortized across the tensors W and A , respectively. As a result the memory access energy is lower and the compute energy is lower during static Ax-BxP. However, for equal re-training effort (5 epochs), the ImageNet accuracy degradation with static Ax-BxP is significantly higher than dynamic Ax-BxP across configurations and networks. The performance benefits with static Ax-BxP are also shown in Figure 15. The performance benefits during static Ax-BxP is greater than dynamic Ax-BxP across networks and Ax-BxP configurations. This is because in static mode, the AxBxP PEs exhibit significant area benefits, which is exploited to achieve higher throughput.

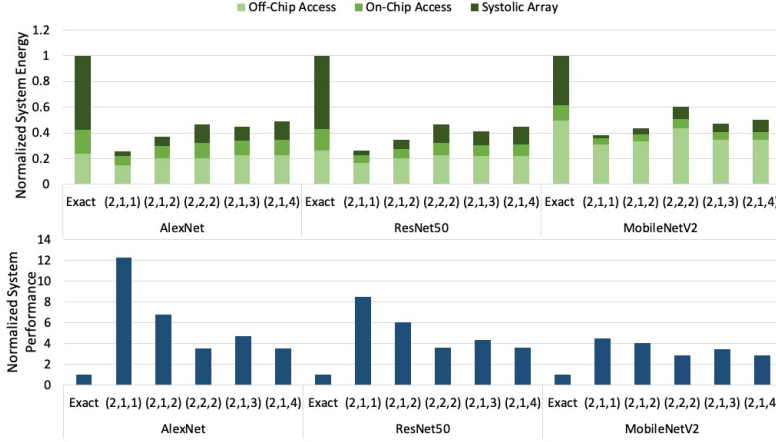


Fig. 14. Ax-BxP Benefits in BitFusion

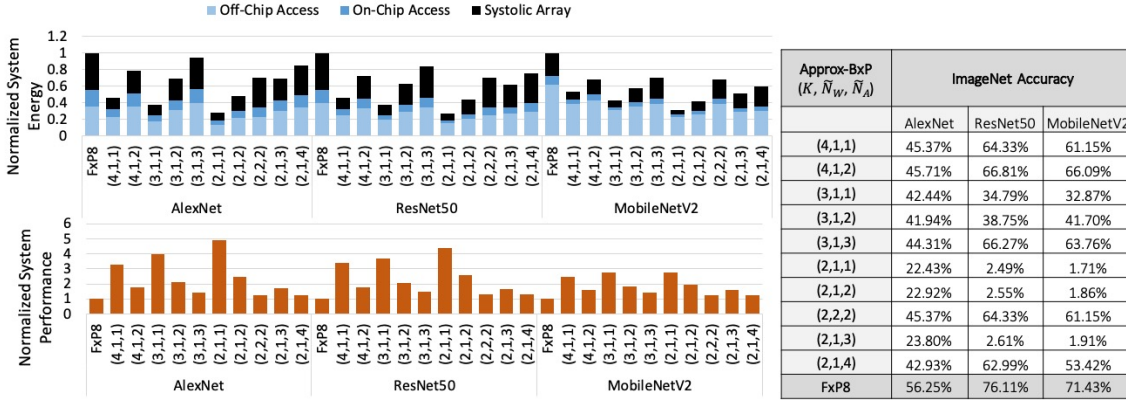


Fig. 15. System-level Benefits with static Ax-BxP

6 RELATED WORK

The high computation and storage demands posed by DNNs have motivated several efforts to focus on precision scaling. Many of the early efforts [21, 24–27] on precision scaling are effective in small networks, but they suffer significant accuracy degradation in large networks.

More recent efforts [8–11, 28, 29] have developed advanced quantization techniques and training methodologies that work well for a wide range of networks and effectively reduce the bit-widths of data-structures to below 8 bits. Notably, PACT [10] has demonstrated successful inference using only 2-bit precision for weights and activations, except in the first and last layers, which are evaluated at 8-bit precision. Other efforts such as BQ [9] and WRPN [8] also achieve adequate inference accuracy using 2-bit weights and activations, by using techniques such as Balanced Quantization and Model scaling respectively. Deep Compression [28] employs a combination of pruning, quantization and Huffman coding to reduce the model size. Bi-Scaled DNN [11] and Compensated DNN [29] leverage the value statistics in DNNs and design number-formats and error compensation schemes that effectively reduce the overall bit-width. Although

these efforts enable DNN inference with ultra-low (below 8-bit) precision, a common precision is not optimal across networks or even across layers within a network. For example, it is a common practice to retain the first and last layers at high precision while quantizing other layers to very low precision in order to preserve accuracy. This fact is further emphasized by works like HAQ [7], which argue that the minimum precision requirement varies within a network, across different layers.

Since varying precision requirements are inherent across DNNs, several efforts [14, 15, 17] have focused on the design of precision re-configurable hardware. BISMO [14] proposes a parallelized bit-serial architecture that offers maximum flexibility in terms of bit-widths it can support. Stripes [15] is a similar work that uses bit-serial hardware design to support variable precision. Albeit offering maximum flexibility, the performance of bit serial hardware is limited by high latency and energy caused by its serial nature. In contrast, fixed-precision hardware needs to be designed to support maximum precision and hence is over-designed for applications with low precision requirement. Instead of performing computations serially at the granularity of bits, BitFusion [17] explores serial computation at the granularity of a group of bits and demonstrates superior energy benefits compared to state-of-the-art bit-serial and fixed-precision accelerators. However, the benefits of BitFusion is limited by its high re-configurability overheads [18]. None of these efforts explore the use of approximations to improve the efficiency of variable-precision hardware. Exploiting the resilience of DNNs to approximations, we propose approximate blocked computation as a next step that is complementary to previous efforts. Computations are performed block-wise, where blocks are a group of bits of fixed length. Our approximation methodology reduces the number of block-wise computations, while maintaining the inference accuracy.

The design of approximate multipliers has been extensively explored in the literature. These efforts can be broadly classified into three categories – efforts that focus on the design of general-purpose approximate circuits, efforts that approximate partial-product accumulation, and efforts that approximate partial product generation. Efforts such as [30–33] focus on general-purpose approximate circuit design using voltage over-scaling and logic simplification techniques. The greedy logic simplification approach used in these methods systematically eliminates circuit components based on the circuit activity profile. However, a more energy-efficient way to eliminate multiplier circuit components is by systematically minimizing the computation and accumulation of partial products.

Energy reduction during partial product accumulation can be achieved by approximate adders [34–36] or by approximate accumulation techniques [37]. While these efforts focus on minimizing the energy consumption of accumulation, we note that the multipliers are the primary sources of energy consumption during MAC operations. Several previous works [38–43] have explored the approximation of partial product generation.

In [38], the authors propose a 2x2 under-designed multiplier block and build arbitrarily large power efficient inaccurate multipliers. The inaccurate 4:2 counter in [39] can effectively reduce the partial product stages of the Wallace multiplier. In [40], the authors substitute multiplication with additions and shift operations by representing the integer operands as logarithms with an error correction factor. The computation sharing multiplier proposed in [41, 42] specifically targets computation re-use in vector-scalar products. Reference [43] proposes an approximate multiplier that performs approximation on only the multiplication of lower-order bits. These efforts achieve only computational energy benefits. In contrast, since our proposed Ax-BxP method minimizes the number of operand blocks used in computation, we achieve savings in terms of memory footprint and memory traffic in addition to computational energy savings. Other efforts such as [44–49] have taken a similar approach.

Operand bit-width truncation to minimize partial product generation is explored by efforts such as [44], [45] and [46]. However, these efforts exhibit poor performance during small bit-width computations. In [47], the authors extract an m-bit segment from an n-bit operand and perform an m-bit ($m < n$) bit multiplication, achieving significant energy

benefits. However the segments must be at least $n/2$ bits long, thus limiting the energy savings. An improvement over [47] is proposed by [48] that reduces the segment size beyond $n/2$ while minimizing error, enabling dynamic range multiplication. However, this approach involves complex-circuitry such as leading one-bit detectors, barrel shifters etc., which introduces considerable delay, area and energy overheads that decrease the approximation benefits. The partial product perforation method proposed by [49] aims at generating fewer partial products by dropping a few bits of one operand during multiplication. Since this approach reduces the bit-width (precision) of just one operand, it does not fully utilize the benefits of precision scaling. Moreover, it requires complex error correction methods that further limit the benefits of approximation method. Additionally, none of the efforts discussed thus far support variable precision computations which we have explored in our work.

Reference [50] proposes dynamic range floating-point (FP) format. However, the area and power cost of supporting FP computations is much higher than fixed-point (FxP) computations. In [29], the authors propose error-compensation techniques for reduced-precision FxP multiplication. A novel number format to represent dual-precision FxP numbers is proposed in [11]. Our proposed Ax-BxP format supports a wide range of precision requirements. It enables efficient re-configurability at the block granularity while minimizing the approximation errors.

7 CONCLUSION

The minimum bit-width requirement varies across and within DNNs to preserve classification accuracy. Optimally supporting such varying precision configurations in DNN accelerators is the challenge addressed by our work. We address this challenge algorithmically and in hardware using our proposed Approximate Blocked Computation method. We demonstrate the effectiveness of our approximation algorithm by exhibiting negligible loss in classification accuracy with ImageNet dataset in state-of-the-art DNNs such as AlexNet, ResNet50 and MobileNetV2. Ax-BxP provides upto 1.73x and 2.04x benefits in system energy and performance respectively, while varying configurations across networks. Further, with varying Ax-BxP configurations at the layer level, we achieve upto 2.42x and 2.95x improvements in system energy and performance, respectively.

ACKNOWLEDGEMENT

This work was supported by C-BRIC, one of six centers in JUMP, a Semiconductor Research Corporation (SRC) program, sponsored by DARPA.

REFERENCES

- [1] J. X. Chen. The evolution of computing: Alphago. *Computing in Science Engineering*, 18(4):4–7, 2016.
- [2] Dario Amodei et al. T. Brown. Language models are few-shot learners. 2020.
- [3] Mingxing Tan and Quoc Le. EfficientNet: Rethinking model scaling for convolutional neural networks. In *Proceedings of the 36th International Conference on Machine Learning*, pages 6105–6114, 2019.
- [4] S. Venkataramani, K. Roy, and A. Raghunathan. Efficient embedded learning for iot devices. In *Asia and South Pacific Design Automation Conference (ASP-DAC)*, pages 308–311, Jan 2016.
- [5] V. Sze, Y. Chen, T. Yang, and J. S. Emer. Efficient processing of deep neural networks: A tutorial and survey. *Proceedings of the IEEE*, 105(12):2295–2329, Dec 2017.
- [6] Doe Hyun et al. N. P. Jouppi. In-datacenter performance analysis of a tensor processing unit. *SIGARCH Comput. Archit. News*, 45(2), 2017.
- [7] Kuan Wang, Zhijian Liu, Yujun Lin, Ji Lin, and Song Han. Haq: Hardware-aware automated quantization with mixed precision. In *Proc. CVPR*, 2019.
- [8] Asit Mishra, Eriko Nurvitadhi, Jeffrey J Cook, and Debbie Marr. Wrpn: wide reduced-precision networks. 2017.
- [9] Shuchang Zhou, Yuzhi Wang, He Wen, Qinyao He, and Yuheng Zou. Balanced quantization: An effective and efficient approach to quantized neural networks. *JCST*, 32(4), 2017.
- [10] Jungwook Choi, Zhuo Wang, Swagath Venkataramani, Pierce I-Jen Chuang, Vijayalakshmi Srinivasan, and Kailash Gopalakrishnan. Pact: Parameterized clipping activation for quantized neural networks. 2018.

- [11] S. Jain, S. Venkataramani, V. Srinivasan, J. Choi, K. Gopalakrishnan, and L. Chang. Biscald-dnn: Quantizing long-tailed datastructures with two scale factors for deep neural networks. In *56th ACM/IEEE Design Automation Conference (DAC)*, pages 1–6, 2019.
- [12] Patrick Judd, Jorge Albericio, Tayler Hetherington, Tor M. Aamodt, Natalie Enright Jerger, and Andreas Moshovos. Proteus: Exploiting numerical precision variability in deep neural networks. In *In Proc. ICS*, 2016.
- [13] Soheil Hashemi, Nicholas Anthony, Hokchhay Tann, R. Iris Bahar, and Sherief Reda. Understanding the impact of precision quantization on the accuracy and energy of neural networks. In *In Proc. DATE*, 2017.
- [14] Yaman Umuroglu, Lahiru Rasnayake, and Magnus Sjalander. Bismo: A scalable bit-serial matrix multiplication overlay for reconfigurable computing. In *ICFPL*. IEEE, 2018.
- [15] P. Judd, J. Albericio, T. Hetherington, T. M. Aamodt, and A. Moshovos. Stripes: Bit-serial deep neural network computing. In *MICRO*. IEEE, 2016.
- [16] Sayeh Sharify, Alberto Delmas Lascorz, Kevin Siu, Patrick Judd, and Andreas Moshovos. Loom: Exploiting weight and activation precisions to accelerate convolutional neural networks. In *DAC*. ACM, 2018.
- [17] Hardik Sharma, Jongse Park, Naveen Suda, Liangzhen Lai, Benson Chau, Joon Kyung Kim, Vikas Chandra, and Hadi Esmaeilzadeh. Bit fusion: Bit-level dynamically composable architecture for accelerating deep neural networks. In *Proc. ISCA*, 2018.
- [18] V. Camus, L. Mei, C. Enz, and M. Verhelst. Review and benchmarking of precision-scalable multiply-accumulate unit architectures for embedded neural-network processing. *IEEE Journal on Emerging and Selected Topics in Circuits and Systems*, 9(4):697–711, 2019.
- [19] Swagath Venkataramani, Ashish Ranjan, Kaushik Roy, and Anand Raghunathan. Axnn: Energy-efficient neuromorphic systems using approximate computing. In *Proceedings of the 2014 International Symposium on Low Power Electronics and Design*, page 27–32, 2014.
- [20] R.I. Hartley and K.K. Parhi. *Digit-Serial Computation*. 1995.
- [21] S.Zhou et al. Dorefa-net: Training low bitwidth convolutional neural networks with low bitwidth gradients. *arXiv preprint arXiv:1606.06160*, 2016.
- [22] Ananda Samajdar, Yuhao Zhu, Paul Whatmough, Matthew Mattina, and Tushar Krishna. Scale-sim: Systolic cnn accelerator. 2019.
- [23] Muralimanohar Naveen; Balasubramonian Rajeev; Jouppi Norman P. Cacti 6.0: A tool to model large caches. Technical report, 2009.
- [24] Fengfu Li, Bo Zhang, and Bin Liu. Ternary weight networks. 2016.
- [25] Itay Hubara, Matthieu Courbariaux, Daniel Soudry, Ran El-Yaniv, and Yoshua Bengio. Quantized neural networks: Training neural networks with low precision weights and activations. *JMLR*, 18(1), 2017.
- [26] Matthieu Courbariaux, Itay Hubara, Daniel Soudry, Ran El-Yaniv, and Yoshua Bengio. Binarynet: Training deep neural networks with weights and activations constrained to+ 1 or- 1. 2016.
- [27] Mohammad Rastegari, Vicente Ordonez, Joseph Redmon, and Ali Farhadi. Xnor-net: Imagenet classification using binary convolutional neural networks. In *Computer Vision – ECCV*. Springer, 2016.
- [28] Song Han, Huizi Mao, and William J. Dally. Deep compression: Compressing deep neural networks with pruning, trained quantization and Huffman coding. 2016.
- [29] S. Jain, S. Venkataramani, V. Srinivasan, J. Choi, P. Chuang, and L. Chang. Compensated-dnn: Energy efficient low-precision deep neural networks by compensating quantization errors. In *55th ACM/ESDA/IEEE Design Automation Conference (DAC)*, pages 1–6, 2018.
- [30] Y. Liu, T. Zhang, and K. K. Parhi. Computation error analysis in digital signal processing systems with overscaled supply voltage. *IEEE Transactions on Very Large Scale Integration (VLSI) Systems*, 18(4):517–526, 2010.
- [31] S. Venkataramani, A. Sabne, V. Kozhikkottu, K. Roy, and A. Raghunathan. Salsa: Systematic logic synthesis of approximate circuits. In *DAC Design Automation Conference 2012*, pages 796–801, 2012.
- [32] Z. Vasicek and L. Sekanina. Evolutionary approach to approximate digital circuits design. *IEEE Transactions on Evolutionary Computation*, 19(3):432–444, 2015.
- [33] R. Venkatesan, A. Agarwal, K. Roy, and A. Raghunathan. Macaco: Modeling and analysis of circuits for approximate computing. In *2011 IEEE/ACM International Conference on Computer-Aided Design (ICCAD)*, pages 667–673, 2011.
- [34] Ajay K. Verma, Philip Brisk, and Paolo Ienne. Variable latency speculative addition: A new paradigm for arithmetic circuit design. In *Proceedings of the Conference on Design, Automation and Test in Europe*, page 1250–1255, 2008.
- [35] Ning Zhu, Wang Ling Goh, Weiya Zhang, Kiat Seng Yeo, and Zhi Hui Kong. Design of low-power high-speed truncation-error-tolerant adder and its application in digital signal processing. *IEEE Transactions on Very Large Scale Integration (VLSI) Systems*, 18(8), 2010.
- [36] V. Gupta, D. Mohapatra, S. P. Park, A. Raghunathan, and K. Roy. Impact: Imprecise adders for low-power approximate computing. In *IEEE/ACM International Symposium on Low Power Electronics and Design*, pages 409–414, 2011.
- [37] I. Qiqieh, R. Shafik, G. Tarawneh, D. Sokolov, and A. Yakovlev. Energy-efficient approximate multiplier design using bit significance-driven logic compression. In *Design, Automation Test in Europe Conference Exhibition (DATE), 2017*, pages 7–12, 2017.
- [38] P. Kulkarni, P. Gupta, and M. Ercegovac. Trading accuracy for power with an underdesigned multiplier architecture. In *2011 24th International Conference on VLSI Design*, pages 346–351, 2011.
- [39] C. Lin and I. Lin. High accuracy approximate multiplier with error correction. In *2013 IEEE 31st International Conference on Computer Design (ICCD)*, pages 33–38, 2013.
- [40] Patricio Bulić Uroš Lotrič. Applicability of approximate multipliers in hardware neural networks. *Neurocomputing*, 96:57–65, 2012.
- [41] Syed Shakib Sarwar, Swagath Venkataramani, Aayush Ankit, Anand Raghunathan, and Kaushik Roy. Energy-efficient neural computing with approximate multipliers. 14, 2018.

- [42] Jongsun Park, Hunsoo Choo, K. Muhammad, SeungHoon Choi, Yonghee Im, and Kaushik Roy. Non-adaptive and adaptive filter implementation based on sharing multiplication. In *2000 IEEE International Conference on Acoustics, Speech, and Signal Processing. Proceedings (Cat. No.00CH37100)*, volume 1, pages 460–463 vol.1, 2000.
- [43] Khaing Yin Kyaw, Wang Ling Goh, and Kiat Seng Yeo. Low-power high-speed multiplier for error-tolerant application. In *2010 IEEE International Conference of Electron Devices and Solid-State Circuits (EDSSC)*, pages 1–4, 2010.
- [44] M. J. Schulte and E. E. Swartzlander. Truncated multiplication with correction constant [for dsp]. In *Proceedings of IEEE Workshop on VLSI Signal Processing*, pages 388–396, 1993.
- [45] S. S. Kidambi, F. El-Guibaly, and A. Antoniou. Area-efficient multipliers for digital signal processing applications. *IEEE Transactions on Circuits and Systems II: Analog and Digital Signal Processing*, 43(2):90–95, 1996.
- [46] Jer Min Jou, Shiann Rong Kuang, and Ren Der Chen. Design of low-error fixed-width multipliers for dsp applications. *IEEE Transactions on Circuits and Systems II: Analog and Digital Signal Processing*, 46(6):836–842, 1999.
- [47] S. Narayanamoorthy, H. A. Moghaddam, Z. Liu, T. Park, and N. S. Kim. Energy-efficient approximate multiplication for digital signal processing and classification applications. *IEEE Transactions on Very Large Scale Integration (VLSI) Systems*, 23(6):1180–1184, 2015.
- [48] S. Hashemi, R. I. Bahar, and S. Reda. Drum: A dynamic range unbiased multiplier for approximate applications. In *2015 IEEE/ACM International Conference on Computer-Aided Design (ICCAD)*, pages 418–425, 2015.
- [49] G. Zervakis, K. Tsoumanis, S. Xydis, D. Soudris, and K. Pekmetzi. Design-efficient approximate multiplication circuits through partial product perforation. *IEEE Transactions on Very Large Scale Integration (VLSI) Systems*, 24(10):3105–3117, 2016.
- [50] J. Y. F. Tong, D. Nagle, and R. A. Rutenbar. Reducing power by optimizing the necessary precision/range of floating-point arithmetic. *IEEE Transactions on Very Large Scale Integration (VLSI) Systems*, 8(3):273–286, 2000.